coatings

MDPI

Communication

Health and Durability of Protective and Thermal Barrier Coatings Monitored in Service by Visual Inspection

Andrzej Szczepankowski, Radoslaw Przysowa *, Jerzy Perczyński and Artur Kułaszka

Instytut Techniczny Wojsk Lotniczych (ITWL), Ul. Ksiecia Boleslawa 6, 01-494 Warsaw, Poland; andrzej.szczepankowski@itwl.pl (A.S.); jerzy.perczynski@itwl.pl (J.P.); artur.kulaszka@itwl.pl (A.K.)
* Correspondence: radoslaw.przysowa@itwl.pl

Abstract: Protective and Thermal Barrier Coatings (TBC) applied on gas-turbine blades gradually degrade due to oxidation, aluminum depletion and impacts of environmental particles. Among various non-destructive coating testing methods (NDT), visual inspection can be undertaken regularly in service, but it provides little quantitative information, and only surface defects can be detected. This work aims at in-service monitoring of turbine blades with multilayer coatings applied by atmospheric plasma spraying (APS) in a few variants. They were validated during a series of accelerated mission tests of a retired military turbofan engine in a test cell together with five other technologies. The fifty-hour rainbow test focused on assessing coating durability. Between engine runs, 12 borescope inspections were conducted to monitor the health of the blades. Finally, the blades were disassembled and examined using computed tomography (CT) and metallographic methods. Throughout the testing, 31 newly-coated blades (66%) withstood the tests, producing results comparable to the reference blades. However, 16 blades suffered intolerable failures observed as increased roughness, gradual loss of the topcoat, spallation and minor foreign object damage. Visual inspection results were generally in agreement with subsequent laboratory tests.

Keywords: military turbofan; turbine blade; protective coatings; thermal barrier coating; thermal spraying; non-destructive testing; visual inspection; maintenance, repair and overhaul (MRO)

Citation: Szczepankowski, A.; Przysowa, R.; Perczyński, J.; Kułaszka, A. Health and Durability of Protective and Thermal Barrier Coatings Monitored in Service by Visual Inspection. *Coatings* **2022**, *12*, 624. https://doi.org/10.3390/coatings12050624

Academic Editor: Shijie Wang

Received: 7 March 2022
Accepted: 29 April 2022
Published: 3 May 2022

1. Introduction

Fuel efficiency is essential for airline competitiveness, while military engine performance determines air superiority. Engine efficiency is directly related to its cycle temperature, which can be increased by using Thermal and Environmental Barrier Coatings, advanced cooling systems and high temperature materials in the hot section. Furthermore, the effectiveness and durability of used coatings determine engine life, availability and maintenance cost.

Gas turbine blades are exposed to high-temperature corrosion and cyclical thermal loads, which lead to surface damage and thermomechanical fatigue [1,2]. The turbine components of the previous engine generations were protected against oxidation by diffusion aluminizing [3–5] and overlay metallic coatings [6,7]. Modern engines use multilayer Thermal Barrier Coatings (TBC), consisting of a metallic bondcoat and a ceramic thermal barrier, most commonly yttria-stabilized zirconia (YSZ). It reduces the operating temperature of the base material (superalloy) by several dozen degrees and thus makes it possible to increase the engine operating temperature and its cycle efficiency. However, when the ceramic layer is damaged, the thermal barrier does not work [8].

Electron Beam Physical Vapor Deposition (EB-PVD) [9,10] was confirmed to be the most effective technology for coating turbine blades as well as the most expensive one. Consequently, manufacturing and repairing coated blades significantly affect the operating cost of the jet engine. Alternatively, cold spraying [11] or thermal spraying methods such as atmospheric plasma spraying (APS) [12,13] can be used. APS is a method that utilizes

a high-energy heat source to melt and accelerate fine particles onto a prepared surface. Metal or ceramic powders can be used in this process to produce protective or thermal barrier layers.

Initially, thermal spray coatings were applied on stationary components (combustion chambers, vanes) [14], whereas PVD methods were used to make coatings on rotating components such as turbine blades. This was due to their higher adhesion and more uniform structure when compared to APS layers. However, coating a blade with APS costs a fraction of a corresponding PVD process since less advanced equipment is necessary and the material is used more effectively. A well-optimized APS process can deliver blade coating that meets the durability requirements. This way, it contributes to reducing the manufacturing cost of turbine blades and also the total cost of the ownership.

To optimize maintenance costs, the user chooses one of the available engine versions, repair contractors and spare parts suppliers. The regeneration of the turbine blades [13,15], including the replacement of the coatings, can be entrusted to one of several contractors who implement their application process. The manufacturing quality, durability and other parameters of blade coatings from different series may differ significantly. It is important to obtain the appropriate thickness, microstructure and layer adhesion. Several well-established methods such as the cyclic oxidation test [9,16], burner-rig test [17] and rainbow test [18,19] are used to evaluate coating durability. Despite advances in the finite element method (FEM) simulation and laboratory tests of blade coatings, aviation regulations still require their final validation in full-scale engine tests.

The common mechanisms of blade coating degradation and failure are: formation of a thermally grown oxides (TGO) on the protective MCrAlY layer [20], initiation and growth of cracks, topcoat thinning and delamination. The topcoat can be spalled due to thermal expansion mismatch, extensive TGO growth or weakening of the binding layer. Each failure mechanism is individual for the type of coating and engine [21–23], and it is essential to understand it to successfully implement a new coating [24,25]. Various non-destructive testing (NDT) [26] methods are used in addition to metallographic examination for quality control in blade production or regeneration. With 3D scanning systems, it is possible to measure the geometry of the uncoated and coated component. After comparing these two datasets numerically, coating thickness can be calculated and visualized [27]. For used blades, the results of their inspection determine the possibility of their reuse. The component regeneration process [28] requires effective methods of assessing the health of the blades and their coatings. Finally, the engine overhaul shop verifies new or refurbished blades usually by visual and fluorescent penetrant inspection (FPI) before they are fitted into the turbine. Only surface defects can be detected visually, whereas FPI can expose most blade cracks [29].

Most classic NDT methods, e.g., eddy current (EC), ultrasonic or even computed tomography (CT), fail to distinguish the base material and MCrAlY (Ni, Co, Cr, Al, Y) coating due to the similarity of materials. EC performs better at measuring the thickness of ceramic layers because they are non-conductive. To test metallic coatings, high-frequency eddy currents of several MHz [30] must be used. Similarly, crack detection and layer thickness measurements can be undertaken with high-frequency 5–25 MHz ultrasound waves [31,32]. Due to complex airfoil geometry (e.g., at LE), the measurements of blade coatings are less accurate than ones on flat surfaces.

CT is an effective tool for the inspection of blades that can be used to measure wall thickness and detect cracks and voids [33,34]. In the case of blade coatings, the CT capabilities are very limited. Contrasting images of coatings can be produced by microtomography, in which a portion of a cooled blade (selected wall, e.g., LE) is scanned close to the detector [35]. One can then roughly measure the thickness of the layer and detect cracks and larger voids [36]. However, it is often necessary to cut this section of the airfoil to expose the coating properly.

Thermophysical properties such as expansion, conductivity and thermal diffusivity determine the durability and technical condition of blade coatings [37,38]. Thus, various

variants of thermography are used to inspect the coatings, such as flash pulsed thermography (PT) [39–42], induction thermography [43] and laser scanning thermography [44,45]. Teraherz waves can also be used to inspect and measure the thickness of coatings [46,47]. For example, Unnikrishnakurup et al. [48] used both PT and Terahertz-Time Domain Spectroscopy (THz-TDS) techniques to determine coating thickness and evaluate the degree of degradation of the thin Air Plasma Sprayed (APS) TBCs.

To reduce maintenance costs, inspections should be conducted near the engine, without removing blades from the disc. Marinetti et al. [49] presented an in situ PT inspection of a power turbine. Although most of the NDT methods must be used outside the engine, thanks to the miniaturization of the probes, it is sometimes possible to inspect blades mounted on the disk with inductive thermography or eddy currents [50]. Some other methods such as fringe projection [50,51] can be used for dimensional control and geometry measurement via the turbine inspection slot. There are some emerging methods to monitor TBC health and measure the component surface temperature in the test cell. It is achieved by embedding thin film thermocouples [52] or doping the coating with thermographic phosphors, which remember the maximum temperature that the material has experienced. This temperature is read by analyzing the laser-excited phosphor emission spectrum [53,54]. However, borescope inspection is still one of a few NDT methods that can be used in service for monitoring coating deterioration, but its results depend on operator performance [55].

This work aims at monitoring gradual coating degradation and detecting blade damage in a rainbow field test by visual inspection. It was part of a large project which had a general goal to develop, validate and implement cost-efficient blade coating technologies for the military turbofan. In this paper, the average mission profile was used to design the accelerated engine test. Coated turbine blades were visually inspected before installing them in the turbine, and twelve times during the test program, before each test day. Collected borescope images were processed to describe and analyze progressing coating damage.

2. Materials and Methods

2.1. Engine

A pair of RD-33 engines is used to propel the Mig-29 fighter, which was designed in the late 1970s and is still operated by the Polish Air Force. Klimov RD-33 is a fourth-generation, twin-rotor turbofan with a bypass ratio of 0.49, an overall pressure ratio of 21:1 and an adjustable supersonic nozzle. Its maximum thrust is 50 kN dry and 81 kN afterburning. It consists of: a supersonic inlet; four-stage axial fan; nine-stage axial compressor; annular combustor; two single-stage axial turbines—high-pressure turbine (HPT) and low-pressure turbine (LPT); mixing chamber; afterburner; and variable-geometry exhaust nozzle.

In the RD-33 engine, the afterburner is not ignited with plugs located behind the turbines. Instead, there is a pilot jet nozzle in the main combustor used only to activate the afterburner. It produces a flame that spreads for six seconds from the combustor along the gas path through both turbines. This solution is called the fire track ('ognevaya dorozhka' in Russian). It ensures reliable ignition at high altitudes in an oxygen-poor atmosphere but also causes intensive overheating of turbine components [56].

The RD-33 engine selected for the rainbow test was produced in 1992 in the Russian Federation with a total service life of 1600 flight hours (FH) and a time between overhaul (TBO) of 350 FH. In 2012, its fourth major overhaul was completed. It had been used by the Air Force until 2018, when LE cracks were found in two HPT blades. Until then, it had completed 1421.3 FH in total and was started 1893 times.

In late 2019, the engine was sent to a repair shop to be modified and reassembled, where all 84 HPT blades were replaced with new ones. It was decided that 37 installed blades were standard, while the remaining 47 blades had newly designed coatings applied by local contractors after removing their original coating. The other modules of the engine were not repaired, so several minor flaws remained in the compressing section and combustor. Then, the engine was assembled and tested twice in the test cell for 1 h and 22 min in

total (Figure 1). It turned out that, throughout the test, the unrepaired compressing section and combustor produced particles which impacted some newly coated turbine blades.

Figure 1. Tested RD-33 engine viewed from the right side.

2.2. HPT Blade

The HP turbine is a single-stage axial turbine that drives the HP compressor. It includes a row of 27 guide vanes, the HPT disc with 84 unshrouded blades (Figure 2) and the bearing system. The design point Turbine Outlet Temperature (TOT) at standard sea-level conditions is 785 ± 5 °C. The corresponding Maximum Turbine Inlet Temperature (TIT) is 1530 K (1257 °C). HPT blades have an internal cooling system without film cooling. They are made of ZhS26 or ZhS32 nickel-based alloys with directional solidification [29,57,58].

The HPT blade's coating is originally made using a MAR-1 or MAR-2 device in a so-called ion-plasma process, which is an implementation of Cathodic arc deposition (Arc-PVD) [59–61]. This is a protective coating only, without a thermal barrier. The airfoil is coated with SDP-2 alloy (Ni-20Cr-12Al-0.5Y), whereas LE has an extra layer of VSDP-16 (Ni-Al-Cr-Y). The overall coating thickness at LE is 75–95 µm. In our previous paper [56], HPT blade health was monitored in service via borescope inspection, and the gradual degradation of the original coating caused by overheating, oxidation and corrosion was presented in macroscale. Bogdan et al. studied the microstucture of five blades with varying degrees of wear [42,57]. They observed coating wear and its gradual degradation. Over time, due to operation at elevated temperatures, aluminum is gradually consumed and thermally grown oxides (TGO) are formed on the outer layer. Its roughness increases since pits, voids and microcracks develop, initiated by corrosion, particle impacts and dynamic stress. Therefore, the TGO layer is prone to progressive spallation and consequently the coating becomes thinner. It gradually loses its protecting properties, and the structure of the base material is eventually weakened. The described degradation process is common for MCrAlY coatings [62–64], but it advances very quickly in this military turbofan due to high thermal stress.

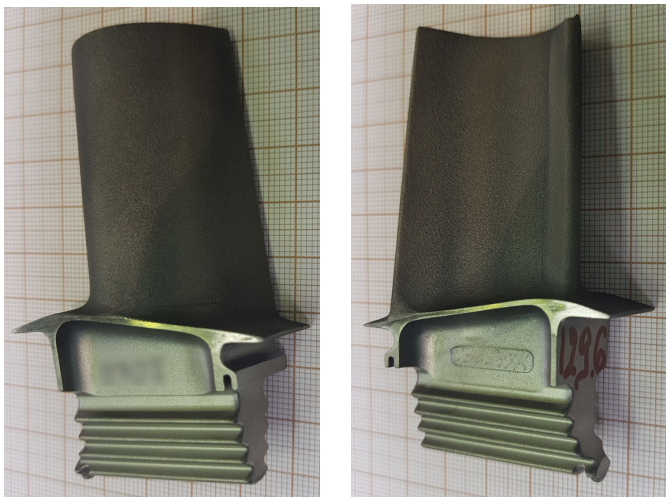

(**a**) (**a**)

Figure 2. HPT blade No 3 coated with APS + VPA. (**a**) Convex side, (**b**) concave side.

2.3. Coatings

APS consists in throwing the molten powder onto the target surface. After hitting the substrate, the molten particle flattens and solidifies very quickly. In this project, Sulzer Metco coating system and AMDRY 386-4 alloy (Table 1) were used. The APS process was optimized to produce MCrAlY and ceramic layers for the HPT turbine blade. The preparation details and microstructure of coated blades were published by Ułanowicz et al. [65]. To obtain the assumed thickness and microstructure of the coating, process parameters such as spraying distance, hydrogen flow, argon flow and the number of the torch passes were modified. The structure, durability and thermal properties of produced specimens were lab-tested to narrow down the number of variants. The development process was then continued for the most promising coating types.

Table 1. Chemical composition of the alloy used in the APS process.

Material	Mass Fraction %						
	Cobalt (Co)	Chrome (Cr)	Aluminum (Al)	Yttrium (Y)	Hafnium (Hf)	Silicon (Si)	Nickel (Ni)
AMDRY 386-4	22	17	12	0.5	0.5	0.4	Base

The selected layers were applied on blades after removing their original coatings in a chemical process [66]. The surface before the spraying was prepared by abrasive blasting with electrocorundum of 60 mesh, at a pressure of 4 bar, from the distance 100–120 mm. Only airfoils were coated, excluding the blade root. After application, the thermal annealing in 1050 °C for 4 h was carried out in vacuum to improve adhesion by diffusion. The target number of coated blades was eight per each technology, but a selected piece was used to create metallographic specimens and further validate the process. Finally, the manufactured blades were inspected visually and installed in the turbine disc following the standard process used for overhauling the engine. Blade selection and placement were performed according to their mass to allow for disc balancing, and consequently, a varying number of blades of each coating type were used.

The experiment in which blades made in several different technologies are fitted on the same disc is often called a rainbow test. Out of ten validated coatings, five types with diffusion, MCrAlY and ceramic layers are presented here (Table 2). Due to confidentiality issues, the other five types are not revealed, but they are listed as 'Other'. Two presented coatings are single layer: CVD (Chemical Vapor Deposition) (B) and APS (E), while the others are double layer. For two-layer coatings, the APS-made MCrAlY bondcoat is

responsible for protection against oxidation and corrosion. The topcoat is either thermal barrier ZrO_2 • Y_2O_3 (G) or a NiAl layer with extra aluminum reserve made in one of the diffusion processes: VPA (Vapor phase aluminide) (C) or SLURRY (F).

The thickness of diffusion layers was 40–70 µm, whereas that of APS-made layers was 60–160 µm. The overall coating thickness was below 160 µm. The coating thickness was controlled by 3D optical scanning and comparing the geometry of the uncoated and coated component [27]. For metallographic specimens, it was measured with Scanning Electron Microscopy (SEM).

Table 2. Number of HPT blades coated with the tested technologies.

Id	Coating Type	Blades	Damaged
A	SDP-2 + VSDP-16	37	0
B	CVD	5	5
C	APS + VPA	8	1
D	Other	4	0
E	APS	6	3
F	APS + SLURRY	5	5
G	APS + TBC	3	2
H	Other	5	0
J	Other	5	0
K	Other	4	0
L	Other	2	0
	Total	84	16

2.4. Engine Testing

Accelerated Mission Testing (AMT), consisting of multiple speed and thermal load cycles, is a known method to reduce the cost and duration of engine durability and endurance testing. In this work, the test program of 50 h was proposed. During the testing, the engine was subjected to dynamic and thermal loads that corresponded to 200 FH. The test profile was designed to represent as far as possible operating modes and maneuvers carried out in normal operation.

There is no counter for LCF engine cycles in Mig-29 because flight hours are the primary measure of engine usage. However, mission data from flight data recorders (FDR) are systematically processed by Polish Air Force to count engine starts, afterburner activations and time of operation at the maximum speed referred to as military power (MIL). These values were aggregated for the whole fleet and averaged to create a mean mission profile. It was found that engine cycles, military power usage and afterburner activations in RD-33 turbofan increase linearly with flight hours with little spread [56]. This is due to a similar mission profile of Polish Mig-29 aircraft and the short TBO of RD-33 engines. Throughout 350 FH, the engine was started 437 times on average, it entered MIL mode 4998 times for 45 FH in total, and it activated the afterburner 773 times (Table 3). Our endurance test was designed to maintain these usage coefficients and reduce the engine operating time from 200 to 50 h. It was achieved by avoiding dwelling at idle or cruise.

The executed test program included 250 test cycles shown in Figure 3. Each engine test-run (equivalent to one test cycle) included 11 thermal cycles at MIL plus two afterburner activations. The bottom part of Table 3 presents planned engine operating time, military power usage and afterburner activations for 1, 5 and 250 cycles.

Table 3. Flight hours versus engine cycles, military power usage and afterburner activations for average engine (row 1–2) and accelerated mission test (row 3–5).

	FH	Cycles	AB	MIL	MIL (FH)	MIL (min)
1	350	437	773	4998	45	2700
2	200	253	440	2818	26	1560
3	50	250	500	2750	25.0	1500
4	1	5	10	55	0.5	30
5	0.2	1	2	11	0.1	6

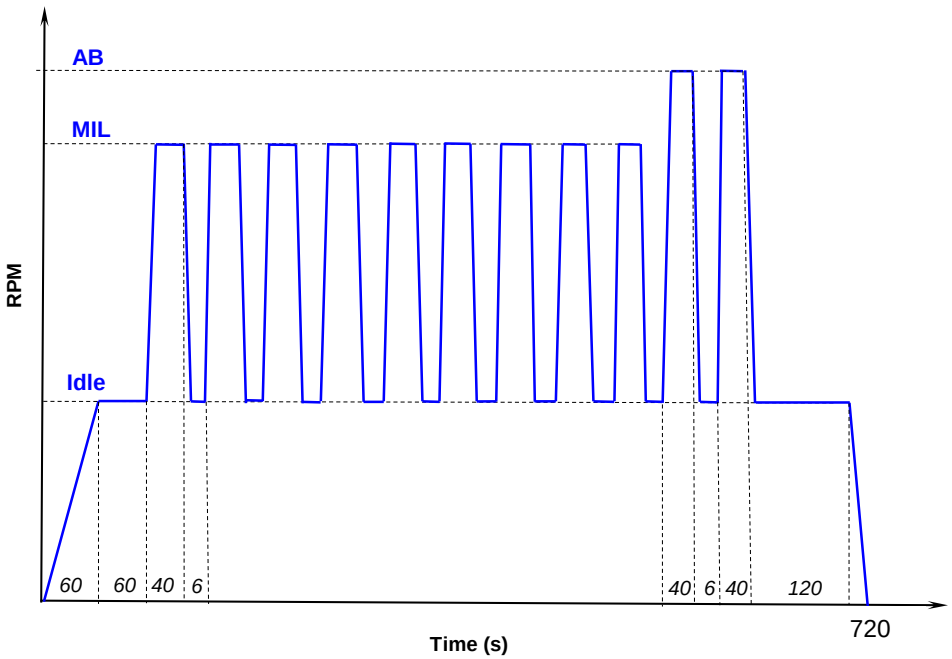

Figure 3. Test cycle proposed for accelerated mission testing.

2.5. Inspection

Both piece-part inspection and borescope inspection were used in this project to check HPT blades. In piece-part inspection, a trained technician checked both sides of the component on the table in the repair shop (Figure 2) before installing it in the turbine disc. He used a magnifying glass and a digital camera to document the inspection. FPI was carried out for the blades for which potential crack symptoms were visible. Two blades with new coatings did not pass the test.

Borescope inspection is periodically carried out in RD-33 turbofans [56], according to technical order 612 [67]. ITWL operates Mentor Visual iQ HD VideoProbe system [68,69] with probes 6.1 mm in diameter, Color SUPER HAD CCD camera of 1.2-megapixel HD image resolution and white LED lighting. In this project, XL4TM61105FG foward view lens was used, with 8-250 mm depth of field and 105 degree field of view.

There are borescope slots in the hot section (Figure 4), two for inspecting the combustor and two others for the turbine. However, there is no direct access to the LE of HPT blades, and the fiber has to enter through the combustor and get closer to the turbine. Individual blades are inspected by manually moving the rotor without changing the position of the fiber, but its head can be flexed if necessary. The example result is presented in Figure 5. In practice, it is hard to obtain a better shot because the view is restricted by the engine design and overlapping adjacent blades. The typical view of HP turbine includes thus a few blades, and the inspected LE takes only a fraction of the HD picture. To evaluate blades, images were rotated and cropped in software to obtain the proper view of LE coating. Due

to the limited resolution of the CCD camera, some pits and minor flaws had dimensions of a few pixels only, so digital magnification was not very useful.

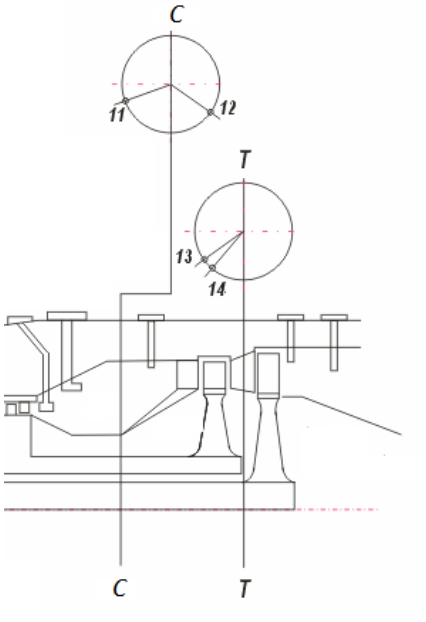

Figure 4. Slots for visual inspections: C—combustor, T—turbine.

Figure 5. C-coated blade 27 viewed through the borescope at the 12th inspection.

A borescope can be modeled as a pinhole camera with a single small aperture. Light rays pass through the aperture and project an inverted image on the camera sensor. Small dimensions of the optical system and limitations in the optimal placing of the sensing head cause significant image distortion. In our previous work [57], MATLAB Computer Vision Toolbox was used to calibrate the borescope system. The determined parameters of the optical system were used for correcting lens distortion, centering the view and automatic image processing. Here, due to limited resolution of the LE representation, we decided to avoid image transformations and let the expert directly analyze the cropped pictures.

In HPT blade evaluation, the applicable requirements were followed. The critical area of the airfoil is the midspan section of LE where no damage except coating discoloration is

allowed by the manufacturer. According to Table 604 in the engine manual [67] (Standard for HPT and LPT turbine damage in point 2-HPT blades), visible erosion, corrosion, melting and delamination of airfoil coatings are not allowed. However, the darkening (discoloration, stains) of the blade airfoils does not indicate failure (point 2.6).

After the engine had performed five test cycles on the first test day, it was inspected the next morning (Table 4). The testing program was completed after 12 test days. During this period, the engine performed 250 test cycles which took 50 h 52 min. In total, it operated for about 52 h and 14 min in the test cell.

Table 4. Daily inspections and engine testing progress.

Test Day	Total Test Hours	Total Test Cycles
1	0	0
2	1 h 52′	5
3	5 h 52′	28
4	11 h 23′	52
5	15 h 01′	72
6	20 h 36′	98
7	26 h 18′	128
8	31 h 44′	155
9	37 h 09′	182
10	41 h 59′	206
11	46 h 38′	229
12	50 h 52′	250

3. Results

This section presents and analyzes the gradual degradation of five new coatings throughout the engine test program. Table 5 includes the failures of coated blades detected at successive inspections. The blades with coating B and G suffered critical damage during a short engine run before the main test cycle and the first inspection, and this is why their operating time to failure is zero.

Table 5. Blade failures—engine operating time and blades in which critical damage was found.

Coating	Blade	Operating Time	Cycles
B	1	0	0
B	7	0	0
B	43	0	0
B	45	0	0
B	47	0	0
C	27	5 h 52′	28
E	11	11 h 23′	52
E	65	11 h 23′	52
E	71	11 h 23′	52
F	13	26 h 18′	128
F	55	15 h 01′	72
F	57	15 h 01′	72
F	61	15 h 01′	72
F	79	26 h 18′	128
G	15	0	0
G	21	0	0

Five damaged blades representing five unsuccessful coatings are presented in Figures 6–10 There are twelve images per figure, showing the results of daily blade inspections with

progressing damage. We present the magnified LE, since it suffers the highest thermal stress and most coating failures start there.

3.1. CVD

Coating B (CVD) was applied to 5 blades (No 1, 7, 43, 45 and 47). The first, noticeable flaws were found during the first inspection (Figure 6). The flaws developed during the initial engine run, before the main test program. During the subsequent test cycles, the destruction of the coating was found to progress in a characteristic way in relation to other tested coatings. The damage was observed on LE along the entire height of the airfoil and on the concave side, especially along the tip and in the trailing edge zone.

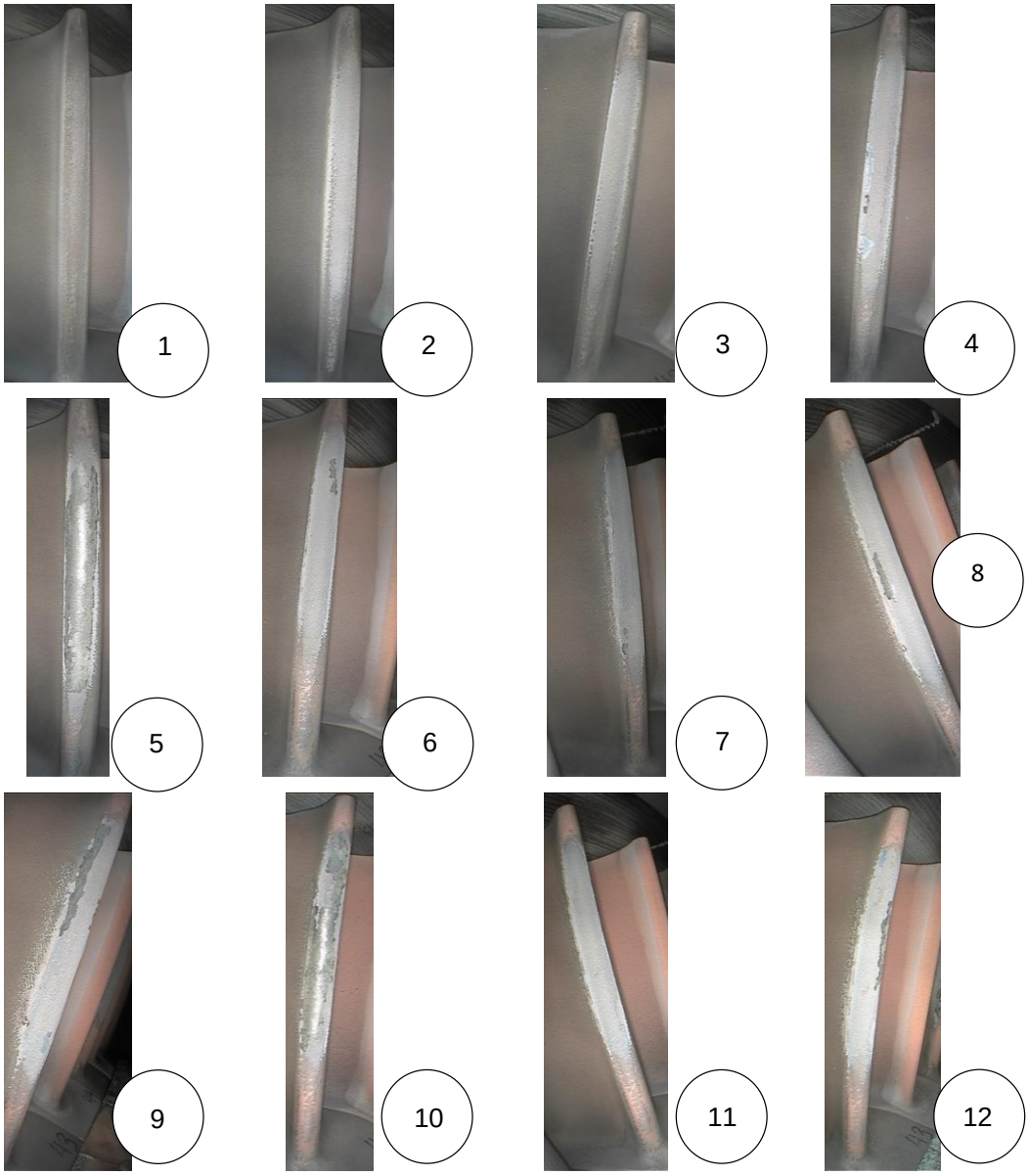

Figure 6. Deterioration of blade 43 observed at successive inspections (1-12).

3.2. APS + VPA

Coating C (APS + VPA) was applied to eight blades, but only blade 27 did not pass the test (Figure 7). During the third inspection, local chipping of the coating from LE was detected. The total area of this defect increased with the number of test cycles so that during the 12th and last inspection, the damage was observed along approximately 60% of the total height of the airfoil. Other C-coated blades were healthy, so it may, for example,

indicate that before the destruction of the LE coating started, blade 27 could have been hit (or rubbed) by a foreign object.

Figure 7. Deterioration of blade 27 observed at successive inspections (1-12).

3.3. APS

Coating E (APS) was put onto six blades, and three of them did not pass the test. Throughout the testing, it was found that the surface roughness increased compared to the standard blades (Figure 8). The leading edges of blades 11, 65 and 71 were damaged. However, the initial deterioration symptoms were found on the LE of the remaining three blades, which were similar to the previous ones. The lack of clear-cut damage symptoms for these three blades may indicate that the applied coating may be, for example, thicker than those on the other three.

The increase in the porosity of the coating at LE observed in subsequent inspections is due to the gradual oxidation of the coating material. This is one of the characteristic symptoms of failure in this type of coating. During the eighth inspection (Figure 8), the appearance of a bond coat at LE (in the midspan of the airfoil) was found. It has also been noticed that the damaged area increases along the height of the blade due to gradual chipping and further oxidation of the material. Thus, this coating is gradually depleted by the hot gas flow. For example, during the last, twelfth inspection, locations at the LE of blade 65 were found which would indicate a complete loss of coating.

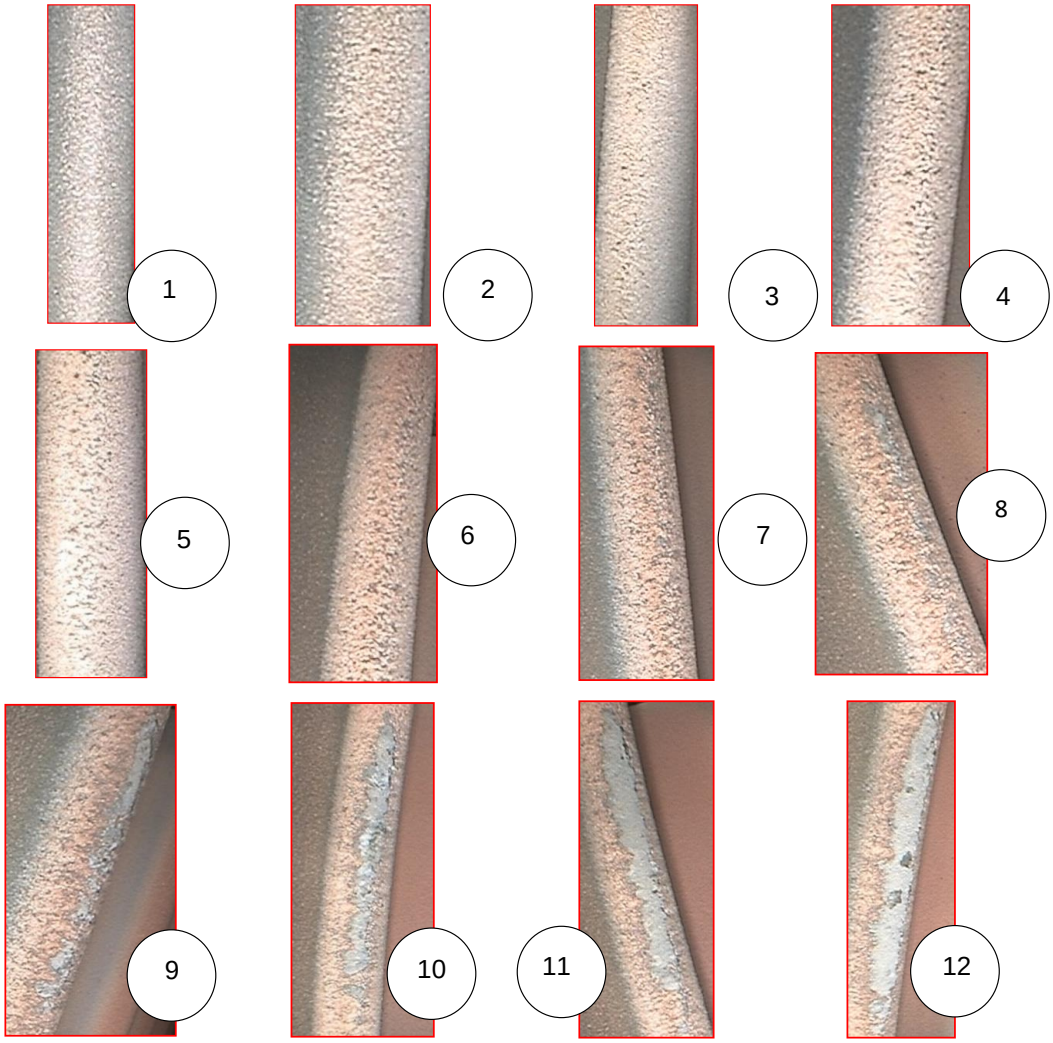

Figure 8. Deterioration of blade 65 observed at successive inspections (1-12).

3.4. APS + SLURRY

Five blades (No 13, 55, 57, 61 and 79) were coated with F coating (APS + SLURRY), and all of them were damaged prior to carrying out 128 of the 250 planned test cycles. During the seventh inspection (after the 128th cycle), local chipping of the LE coating was found in the midspan of blade 13 (Figure 9). Throughout subsequent inspections, an increase in the total area of the wound (along the height of the airfoil) was observed as a result of the gradual chipping of the material.

What is characteristic of this type of coating is that it is damaged locally via the formation of several LE flaws, which are separated (blade 13) or gradually merge, after some test cycles (other F-coated blades). Another characteristic feature of this damage is the fact that the first noticeable flaws occur at the LE arc where the concave side starts. The LE flaws observed later at the point of transition to the convex side are located slightly above those previously identified.

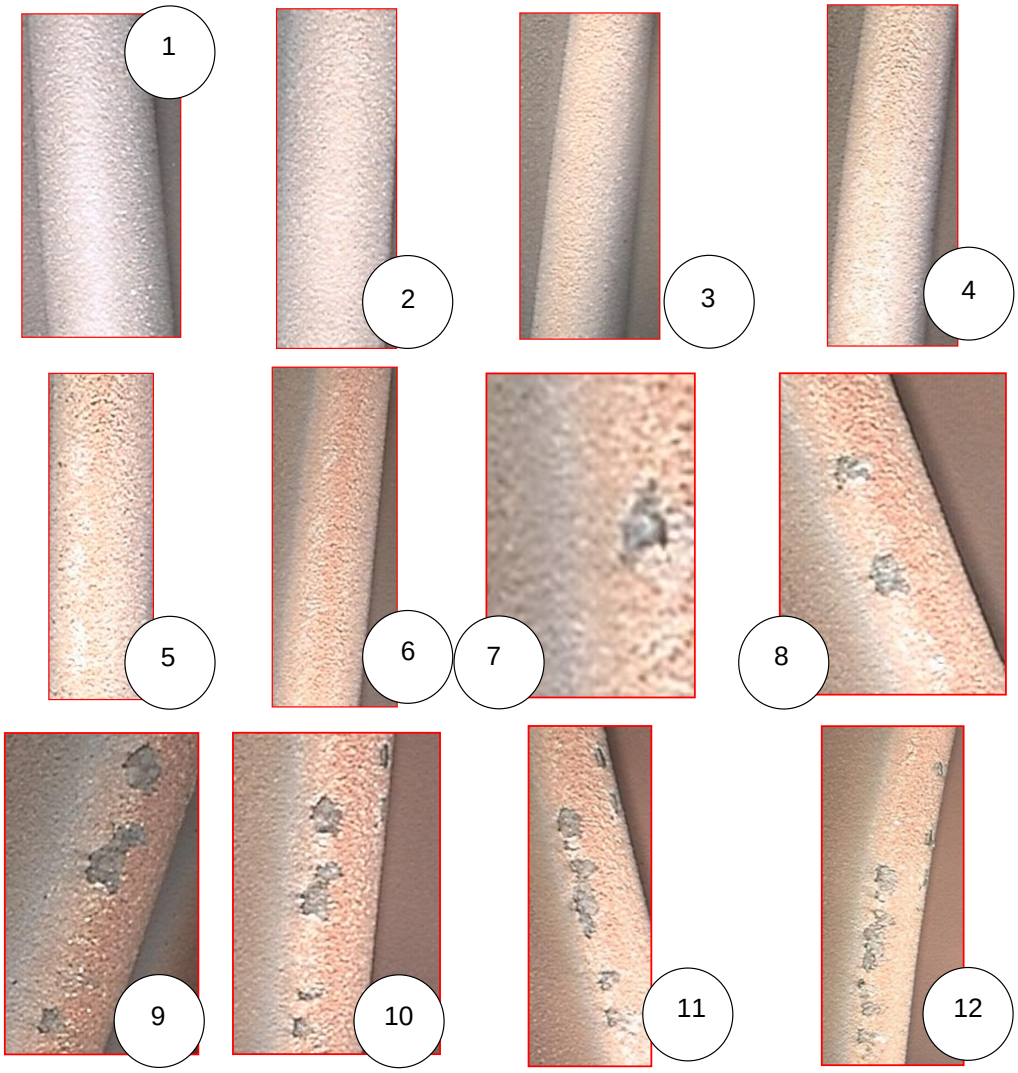

Figure 9. Deterioration of blade 13 (APS + SLURRY) observed at successive inspections (1-12).

3.5. APS + TBC

Coating G (APS + TBC) was applied to three blades (15, 17 and 21), and two did not pass the test. During the verification of the blades before their installation in the disc, minor flaws of the ceramic topcoat were found in blades 17 and 21 at their LEs, in the near-edge zone, both on the concave and convex side. The second inspection revealed an increase in the total area of coating damage in blade 15 along its height (Figure 10). This process accelerated, as during the fourth inspection, the LE of this blade was found to have no coating along the entire height of the blade.

The LE coating of blade 21 declined slightly differently, because apart from an increase in its surface porosity, no other changes were observed until the 11th inspection. Then, a local loss of coating was found in the lower part of the airfoil. The flaw area gradually increased during the 12th (final) test cycle.

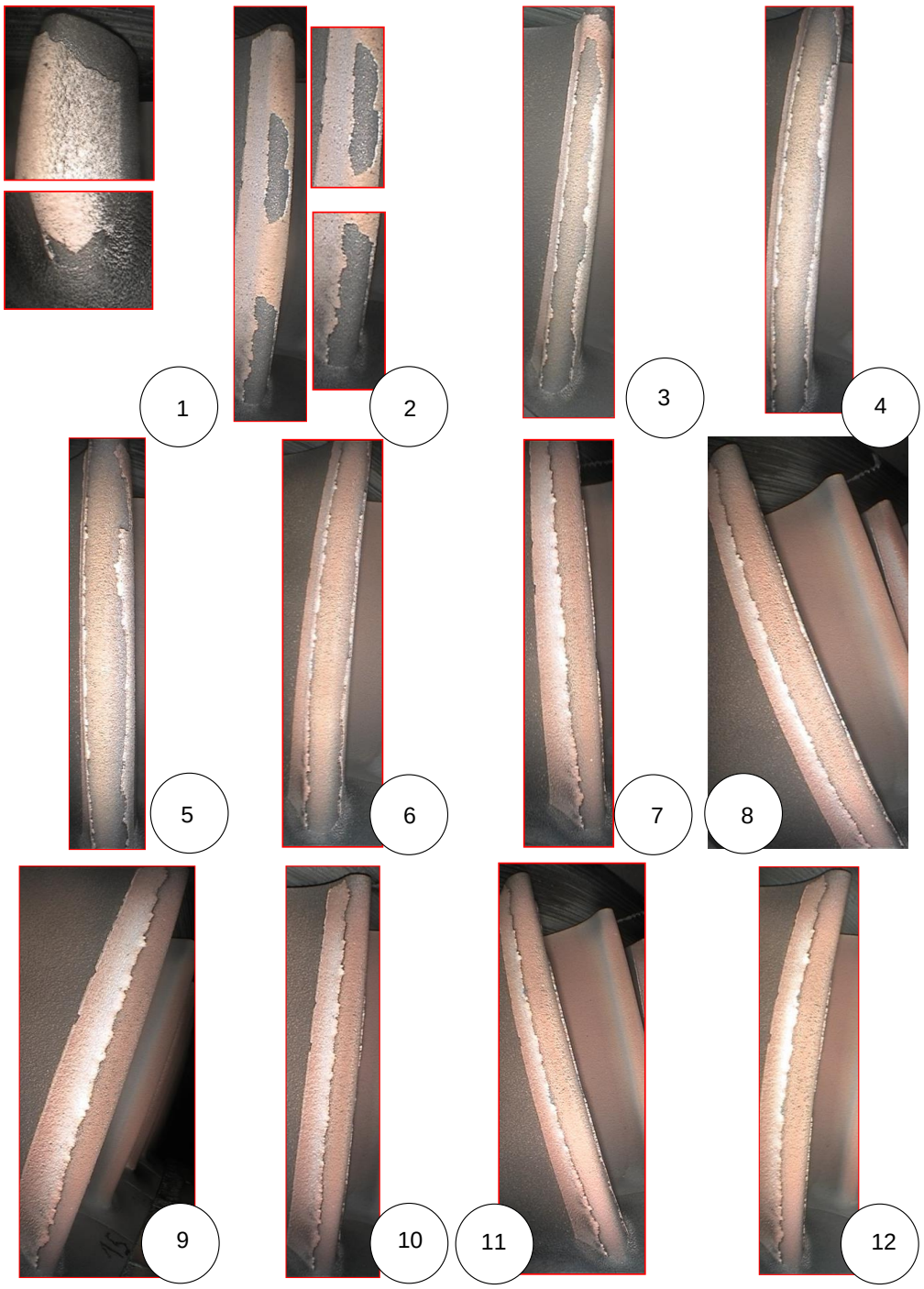

Figure 10. Deterioration of blade 15 (APS + TBC) observed at successive inspections (1-12).

4. Discussion

In this work, the methods for engine testing and visual inspection of coated blades are presented. We confirmed that a borescope system is an effective tool for evaluating coating health at the macroscale. It outperforms a naked eye, magnifying glass and consumer digital camera, since its optical zoom is comparable to simple microscopes. However, it has significant limitations related to restricted access to the component, image distortion and the limited resolution of the CCD camera. Moreover, some images may be difficult to interpret as the lighting provided by the integrated LED diode was absorbed differently by individual coatings [55]. Despite these difficulties, we detected increased roughness, corrosion pits, cracks, gradual loss of the topcoat, spallation and foreign object damage (FOD).

The proposed blade evaluation methodology can be used for standard and newly developed coatings, but it is effective only in detecting macroscale flaws on the airfoil surface. Early stages of coating damage are related to microstructural phenomena and thus cannot be observed with borescope systems or another visual inspection method. However, when the coating damage advances, its symptoms usually can be detected on the blade surface.

The accelerated engine test was designed according to the average mission profile. The adopted test program could only partially simulate 200 FH, but it was sufficient to verify coating technologies and observe the gradual degradation of 16 blades with five new coatings. Numerous transient modes and afterburner activations during the engine test caused dynamic stress and thermal shocks during which the rate of temperature change is as high as a few hundred degrees per second. Such conditions most probably generated microcracks and caused coating delamination.

Preliminary blade testing results are presented here from the perspective of the user who needs to optimize engine repair costs and has a limited set of NDT methods to monitor the health of coated blades. The completed engine test was successful since 31 newly-coated blades (66%) made in eight technologies withstood the tests, producing results comparable to 37 reference blades. The remaining 16 blades made in five technologies suffered intolerable damage. Among five presented coating types, APS + VPA (C) performed best, while B demonstrated insufficient maturity because they spalled during the first engine run. However, more information on the individual technologies is necessary for their detailed comparison and the further evaluation of their durability.

The capability for detecting surface damage and observing progressing coating degradation was demonstrated. Among others, it was shown that the mechanism and pace of failure were specific to the type of coating. However, explaining the damage is not possible without metallographic analysis and studying underlying microstructural phenomena. Based on prior experience, we can presume that the presented coating failures were caused, among others, by the incompatibility of thermal expansion coefficients, insufficient adhesion, binding layer oxidation or the impact of airborne particles. The most common coating defects were found on the leading edge, but no symptom of weakening of the base material was observed in the post-test CT results. Since coatings and their flaws are hardly visible on tomograms, they are not included here.

The engine was operated for 52 h and 14 min in the test cell, performing 250 test cycles in 12 days. The leading edges of 16 blades were found damaged halfway through the testing as soon as the 128th cycle was completed. Moreover, excessive chipping of the material was observed along their tips on the concave side and along the trailing edge. During subsequent test cycles, local coating flaws appeared in the presented blades, and they gradually grew due to the impact of the varying temperature field and other stress. The gathered information on coating degradation will be used by coating designers to improve the deposition process and increase blade durability. It can be also valuable to maintainers who assess the condition of turbines and make go/no-go decisions.

It was found that five B-coated blades and five F-coated blades degraded gradually with the number of test cycles performed (Table 5). The same was true for half of the six blades with coating E. Two of the three G-coated blades were damaged before installing them in the turbine disk, and during engine testing, they underwent further destruction. On the other hand, one of the eight blades with a C layer could have been damaged as a result of an earlier collision with a foreign object, which resulted in the loss of the coat. This confirms that blade coatings are sensitive to minor impacts and other mechanical damage that can occur at any stage of blade preparation, i.e., coating application, blade shipment and their installation in the turbine disc. Therefore, care should be taken to organize the process in a way that excludes the possibility of initiating damage to the coatings.

5. Conclusions

In this work, selected variants of coating processes were tested in the real engine, and thus, causing damage to some of the blades was desirable.

- Despite its limitations, borescope inspection is one of the few tools available for the in-service monitoring of blade coatings.
- The observed pace and mechanism of degradation were specific to the type of coating.
- APS is a cost-effective technology that can replace PVD methods on turbine blades when the proper coating structure and adhesion are ensured.
- The presence of damage at this stage of development is not a problem, and it absolutely does not exclude any of the tested processes.

The collected data on progressing damage along with metallographic analysis of the blades will help to optimize the deposition process and to select the best technology. The laboratory tests, microstructure and failure analysis of tested coatings will be presented in a separate publication. We hope that the coatings developed in this project will be matured and implemented by the industry. For more effective blade inspection in our future coating maturation programs, we plan to employ new-generation borescope systems and digital image processing or other emerging NDT methods.

Author Contributions: Conceptualization, A.S., A.K. and R.P.; methodology, A.S. and A.K.; validation, A.K. and R.P.; investigation, J.P. and A.S.; data curation, J.P. and A.S.; writing—original draft preparation, A.S. and R.P.; writing—review and editing, R.P.; visualization, A.S.; supervision, A.K.; project administration, A.K. All authors have read and agreed to the published version of the manuscript.

Funding: This research was funded by the National Centre for Research and Development, grant number DOB-BIO8/04/01/2016, within the project entitled 'Coatings with increased heat resistance on the high pressure turbine blades of the RD-33 engines'.

Institutional Review Board Statement: Not applicable.

Informed Consent Statement: Not applicable.

Data Availability Statement: Data are contained within the article.

Conflicts of Interest: The authors declare no conflict of interest.

Abbreviations

The following abbreviations are used in this manuscript:

AB	Afterburner
AMT	Accelerated mission test
APS	Atmospheric plasma spraying
CCD	Charge-coupled device
CVD	Chemical Vapor Deposition
CT	Computed tomography
EB-PVD	Electron Beam Physical Vapor Deposition
FH	Flight hours
HPT	High pressure turbine
ITWL	The Air Force Institute of Technology in Warsaw
MIL	Military power
LE	Leading edge
LED	Light-emitting diode
LPT	Low pressure turbine
PVD	Physical Vapor Deposition
SEM	Scanning Electron Microscopy
TBC	Thermal barrier coating
TBO	Time between overhauls
TGO	Thermally grown oxides
TE	Trailing edge
VPA	Vapor phase aluminide

References

1. Ozgurluk, Y.; Doleker, K.M.; Ozkan, D.; Ahlatci, H.; Karaoglanli, A.C. Cyclic hot corrosion failure behaviors of EB-PVD TBC systems in the presence of sulfate and vanadate molten salts. *Coatings* **2019**, *9*, 166. https://doi.org/10.3390/coatings9030166.
2. Song, D.; Song, T.; Paik, U.; Lyu, G.; Jung, Y.G.; Choi, B.G.; Kim, I.S.; Zhang, J. Crack-growth behavior in thermal barrier coatings with cyclic thermal exposure. *Coatings* **2019**, *9*, 365. https://doi.org/10.3390/coatings9060365.
3. Kopec, M.; Kukla, D.; Yuan, X.; Rejmer, W.; Kowalewski, Z.L.; Senderowski, C. Aluminide Thermal Barrier Coating for High Temperature Performance of MAR 247 Nickel Based Superalloy. *Coatings* **2021**, *11*, 48. https://doi.org/10.3390/coatings11010048.
4. Goral, M.; Pytel, M.; Ochal, K.; Drajewicz, M.; Kubaszek, T.; Simka, W.; Nieuzyla, L. Microstructure of aluminide coatings modified by Pt, Pd, Zr and Hf formed in low-activity CVD process. *Coatings* **2021**, *11*, 421. https://doi.org/10.3390/coatings11040421.
5. Kościelniak, B.; Chmiela, B.; Sozańska, M.; Swadźba, R.; Drajewicz, M. Oxidation Behavior of Inconel 740H Nickel Superalloy in Steam Atmosphere at 750 °C. *Materials* **2021**, *14*, 4536. https://doi.org/10.3390/ma14164536.
6. Tamarin, Y. *Protective Coatings for Turbine Blades*; ASM International: Materials Park, OH, USA, 2002; p. 247.
7. Mishra, R.K.; Kumar, P.; Muduli, S.K. Failure Prevention of Gas Turbine Blades Through Pack Aluminization. *J. Fail. Anal. Prev.* **2018**, *18*, 1120–1126. https://doi.org/10.1007/s11668-018-0498-1.
8. Maricocchi, A.; Bartz, A.; Wortman, D. PVD TBC experience on GE aircraft engines. *J. Therm. Spray Technol.* **1997**, *6*, 193–198. https://doi.org/10.1007/s11666-997-0012-x.
9. Swadźba, R.; Wiedermann, J.; Hetmańczyk, M.; Swadźba, L.; Mendala, B.; Witala, B.; Komendera, Ł. Microstructure degradation of EB-PVD TBCs on Pd-Pt-modified aluminide coatings under cyclic oxidation conditions. *Surf. Coat. Technol.* **2013**, *237*, 16–22. https://doi.org/10.1016/j.surfcoat.2013.09.022.
10. Ebach-Stahl, A.; Schulz, U.; Swadźba, R.; Munawar, A.U. Lifetime improvement of EB-PVD 7YSZ TBCs by doping of Hf or Zr in NiCoCrAlY bond coats. *Corros. Sci.* **2021**, *181*, 109205. https://doi.org/10.1016/j.corsci.2020.109205.
11. Guo, D.; Wang, Y.; Fernandez, R.; Zhao, L.; Jodoin, B. Cold spray for production of in-situ nanocrystalline MCrAlY coatings – Part I: Process analysis and microstructure characterization. *Surf. Coatings Technol.* **2021**, *409*, 126854. https://doi.org/10.1016/j.surfcoat.2021.126854.
12. Li, X.; Peng, X.Y.; Dong, H.; Zhou, Y.; Wang, T.; Ren, K.; Sun, L. The Evaluation of Durability of Plasma-Sprayed Thermal Barrier Coatings with Double-layer Bond Coat. *Coatings* **2019**, *9*, 241. https://doi.org/10.3390/coatings9040241.
13. Nicolaus, M.; Möhwald, K.; Maier, H.J. Thermally Sprayed Nickel-Based Repair Coatings for High-Pressure Turbine Blades: Controlling Void Formation during a Combined Brazing and Aluminizing Process. *Coatings* **2021**, *11*, 725. https://doi.org/10.3390/coatings11060725.
14. Liebert, C.H.; Levine, S.R. *Further Industrial Tests of Ceramic Thermal-Barrier Coatings*; NASA Technical Paper 2057; NASA Lewis Research Center Cleveland, OH, USA, 1982;
15. Savinkin, V.V.; Vizureanu, P.; Sandu, A.V.; Ratushnaya, T.Y.; Ivanischev, A.A.; Surleva, A. Improvement of the turbine blade surface phase structure recovered by plasma spraying. *Coatings* **2020**, *10*, 62. https://doi.org/10.3390/coatings10010062.
16. Ghadami, F.; Davoudabadi, M.A.; Ghadami, S. Cyclic Oxidation Properties of the Nanocrystalline AlCrFeCoNi High-Entropy Alloy Coatings Applied by the Atmospheric Plasma Spraying Technique. *Coatings* **2022**, *12*, 372. https://doi.org/10.3390/coatings12030372.
17. Yun, J.; Kim, Y.; Lee, J.M.; Song, H.; Wee, S.; Koo, J.M.; Lee, Y.Z.; Seok, C.S. The Study on Delamination Life of TBC through Burner-Rig Test. *Int. J. Precis. Eng. Manuf.* **2017**, *18*, 555–560. https://doi.org/10.1007/s12541-017-0066-8.
18. Shahoo, P.; Sobieski, P.A. Performance Characteristics of Thermal Barrier Coatings: A Case Study. In Proceedings of the ASME Turbo Expo 2007: Power for Land, Sea and Air, Montreal, QC Canada, 14–17 May 2007; Volume 5, pp. 191–197. https://doi.org/10.1115/GT2007-28352.
19. Witz, G.; Schaudinn, M.; Sopka, J.; Buecklers, T. Development of Advanced Thermal Barrier Coatings with Improved Temperature Capability. In Proceedings of the ASME Turbo Expo 2016: Turbomachinery Technical Conference and Exposition, Seoul, Korea, 13–17 June 2016; Volume 6: Ceramics; Controls, Diagnostics and Instrumentation; Education; Manufacturing Materials and Metallurgy; V006T21A006. pp. 1–8. https://doi.org/10.1115/GT2016-57425.
20. Ghadami, F.; Sabour Rouh Aghdam, A.; Ghadami, S. Microstructural characteristics and oxidation behavior of the modified MCrAlX coatings: A critical review. *Vacuum* **2021**, *185*, 109980. https://doi.org/10.1016/j.vacuum.2020.109980.
21. Hu, Z.C.; Liu, B.; Wang, L.; Cui, Y.H.; Wang, Y.W.; Ma, Y.D.; Sun, W.W.; Yang, Y. Research Progress of Failure Mechanism of Thermal Barrier Coatings at High Temperature via Finite Element Method. *Coatings* **2020**, *10*, 732. https://doi.org/10.3390/coatings10080732.
22. Chang, S.; Oh, K.Y. Contribution of High Mechanical Fatigue to Gas Turbine Blade Lifetime during Steady-State Operation. *Coatings* **2019**, *9*, 229. https://doi.org/10.3390/coatings9040229.
23. Wei, Z.Y.; Cai, H.N. Understanding the Failure Mechanism of Thermal Barrier Coatings Considering the Local Bulge at the Interface between YSZ Ceramic and Bond Layer. *Materials* **2021**, *15*, 275. https://doi.org/10.3390/ma15010275.
24. Kumar, S.; Kant, S.; Suri, N.M.; Verma, R. Effects of Thermal Barrier Coatings on Diesel and Gas turbine engines: A review. *Int. Res. J. Eng. Technol.* **2016**, *3*, 134–139.
25. Abdul-Aziz, A.; Wroblewski, A. Durability Analysis and Experimental Validation of Environmental Barrier Coating (EBC) Performance Using Combined Digital Image Correlation and NDE. *Coatings* **2016**, *6*, 70. https://doi.org/10.3390/coatings6040070.

26. Mevissen, F.; Meo, M. A Review of NDT/Structural Health Monitoring Techniques for Hot Gas Components in Gas Turbines. *Sensors* **2019**, *19*, 711. https://doi.org/10.3390/s19030711.
27. Moskal, G.; Swadźba, R.; Witala, B. Non-Destructive Measurement of Top Coat Thickness in TBC Systems by 3D Optical Topometry. *Nondestruct. Test. Eval.* **2015**, *30*, 39–48. https://doi.org/10.1080/10589759.2014.984297.
28. Aschenbruck, J.; Adamczuk, R.; Seume, J.R. Recent Progress in Turbine Blade and Compressor Blisk Regeneration. *Procedia CIRP* **2014**, *22*, 256–262. https://doi.org/10.1016/j.procir.2014.07.016.
29. Kukla, D.; Kopec, M.; Sitek, R.; Olejnik, A.; Kachel, S.; Kiszkowiak, Ł. A Novel Method for High Temperature Fatigue Testing of Nickel Superalloy Turbine Blades with Additional NDT Diagnostics. *Materials* **2021**, *14*, 1392. https://doi.org/10.3390/ma14061392.
30. Bruchwald, O.; Nicolaus, M.; Frackowiak, W.; Reimche, W.; Möhwald, K.; Maier, H.J. Material characterization of thin coatings using high frequency eddy current technology. In Proceedings of the 19th World Conference on Non-Destructive Testing (WCNDT 2016), Munich, Germany, 13–17 June 2016; pp. 1–6.
31. Chen, H.L.R.; Zhang, B.; Alvin, M.A.; Lin, Y. Ultrasonic Detection of Delamination and Material Characterization of Thermal Barrier Coatings. *J. Therm. Spray Technol.* **2012**, *21*, 1184–1194. https://doi.org/10.1007/s11666-012-9811-9.
32. Zhang, S.; Lv, G.; Guo, S.; Zhang, Y.; Feng, W. Porosity Characterization of Thermal Barrier Coatings by Ultrasound with Genetic Algorithm Backpropagation Neural Network. *Complexity* **2021**, *2021*, 8869928. https://doi.org/10.1155/2021/8869928.
33. Hastie, S.; Chan, A.; Wiens, K.; Nagy, D.; Tollett, R.; Lowden, P. Computed Tomography Wall Thickness Inspection to Support Gas Turbine Blade Life Extension. In Proceedings of the ASME Turbo Expo 2021: Turbomachinery Technical Conference and Exposition, Virtual, 7–11 June 2021; V007T17A021, American Society of Mechanical Engineers: Huston, TX, USA 2021; Volume 7: Industrial and Cogeneration; Manufacturing Materials and Metallurgy. https://doi.org/10.1115/GT2021-60316.
34. Przysowa, R.; Chalimoniuk, M.; Grzelka-Gajek, D.; Shakalo, R.; Karpenko, A. CT Inspection of Cooled Turbine Blades. *J. KONBiN* **2020**, *50*, 307–331. https://doi.org/10.2478/jok-2020-0064.
35. Zhao, Y.; Shinmi, A.; Zhao, X.; Withers, P.J.; Van Boxel, S.; Markocsan, N.; Nylen, P.; Xiao, P. Investigation of Interfacial Properties of Atmospheric Plasma Sprayed Thermal Barrier Coatings with Four-Point Bending and Computed Tomography Technique. *Surf. Coat. Technol.* **2012**, *206*, 4922–4929. https://doi.org/10.1016/j.surfcoat.2012.05.099.
36. Błachnio, J.; Chalimoniuk, M.; Kułaszka, A.; Borowczyk, H.; Zasada, D. Exemplification of Detecting Gas Turbine Blade Structure Defects Using the X-ray Computed Tomography Method. *Aerospace* **2021**, *8*, 119. https://doi.org/10.3390/aerospace8040119.
37. Panas, A.J.; Senderowski, C.; Fikus, B. Thermophysical properties of multiphase Fe-Al intermetallic-oxide ceramic coatings deposited by gas detonation spraying. *Thermochim. Acta* **2019**, *676*, 164–171. https://doi.org/10.1016/j.tca.2019.04.009.
38. Curry, N.; VanEvery, K.; Snyder, T.; Markocsan, N. Thermal conductivity analysis and lifetime testing of suspension plasma-sprayed thermal barrier coatings. *Coatings* **2014**, *4*, 630–650. https://doi.org/10.3390/coatings4030630.
39. Ptaszek, G.; Cawley, P.; Almond, D.; Pickering, S. Artificial Disbonds for Calibration of Transient Thermography Inspection of Thermal Barrier Coating Systems. *NDT E Int.* **2012**, *45*, 71–78. https://doi.org/10.1016/j.ndteint.2011.09.008.
40. Kidd, G.; Nunn, J. Application of Pulsed Thermography to Quality Assurance of Thermal Barrier Coatings. *Proc. Inst. Mech. Eng. Part G J. Aerosp. Eng.* **2012**, *226*, 873–880. https://doi.org/10.1177/0954410011414312.
41. Chung, Y.; Lee, S.; Kim, W. Latest Advances in Common Signal Processing of Pulsed Thermography for Enhanced Detectability: A Review. *Appl. Sci.* **2021**, *11*, 12168. https://doi.org/10.3390/app112412168.
42. Bogdan, M.; Błachnio, J.; Spychała, J.; Zasada, D. Assessment of usability of the exploited gas turbine blade heat-resistant coatings. *Eng. Fail. Anal.* **2019**, *105*, 337–346. https://doi.org/10.1016/j.engfailanal.2019.07.016.
43. Wang, Y.; Gao, X.; Netzelmann, U. Detection of Surface Cracks in Metals under Coatings by Induction Thermography. In Proceedings of the 2018 International Conference on Quantitative InfraRed Thermography, QIRT Council, Berlin, Germany, 25–29 June 2018; pp. 602–611. https://doi.org/10.21611/qirt.2018.064.
44. Liu, Z.; Jiao, D.; Shi, W.; Xie, H. Linear Laser Fast Scanning Thermography NDT for Artificial Disbond Defects in Thermal Barrier Coatings. *Opt. Express* **2017**, *25*, 31789. https://doi.org/10.1364/oe.25.031789.
45. Muzika, L.; Svantner, M.; Honner, M.; Houdkova, S. Laser Scanning Thermography for Coating Thickness Inspection. *Eng. Proc.* **2021**, *8*, 17. https://doi.org/10.3390/engproc2021008017.
46. Fukuchi, T.; Ozeki, T.; Okada, M.; Fujii, T. Nondestructive Inspection of Thermal Barrier Coating of Gas Turbine High Temperature Components. *IEEJ Trans. Electr. Electron. Eng.* **2016**, *11*, 391–400. https://doi.org/10.1002/tee.22255.
47. Isern, L.; Waddie, A.J.; Chalk, C.; Moore, A.J.; Nicholls, J.R. Non-Destructive Thickness Measurement of Thermal Barrier Coatings Using Terahertz Radiation. *Emergent Mater.* **2021**, *4*, 1547–1557. https://doi.org/10.1007/s42247-021-00275-6.
48. Unnikrishnakurup, S.; Dash, J.; Ray, S.; Pesala, B.; Balasubramaniam, K. Nondestructive Evaluation of Thermal Barrier Coating Thickness Degradation Using Pulsed IR Thermography and THz-TDS Measurements: A Comparative Study. *NDT E Int.* **2020**, *116*, 102367. https://doi.org/10.1016/j.ndteint.2020.102367.
49. Marinetti, S.; Robba, D.; Cernuschi, F.; Bison, P.G.; Grinzato, E. Thermographic Inspection of TBC Coated Gas Turbine Blades: Discrimination between Coating over-Thicknesses and Adhesion Defects. *Infrared Phys. Technol.* **2007**, *49*, 281–285. https://doi.org/10.1016/j.infrared.2006.06.018.
50. Frackowiak, W.; Barton, S.; Reimche, W.; Bruchwald, O.; Zaremba, D.; Schlobohm, J.; Li, Y.; Kaestner, M.; Reithmeier, E. Near-Wing Multi-Sensor Diagnostics of Jet Engine Components. In Proceedings of the ASME Turbo Expo 2018: Turbomachinery Technical Conference and Exposition, Oslo, Norway, 11–15 June 2018; American Society of Mechanical Engineers: Huston, TX, USA, 2018;

Volume 6: Ceramics; Controls, Diagnostics, and Instrumentation; Education; Manufacturing Materials and Metallurgy; pp. 1–8. https://doi.org/10.1115/GT2018-76793.
51. Schlobohm, J.; Bruchwald, O.; Frąckowiak, W.; Li, Y.; Kästner, M.; Pösch, A.; Reimche, W.; Maier, H.J.; Reithmeier, E. Advanced Characterization Techniques for Turbine Blade Wear and Damage. *Procedia CIRP* **2017**, *59*, 83–88. https://doi.org/10.1016/j.procir.2016.09.005.
52. Yang, D.; Pankov, V.; Zhao, L.; Patnaik, P. Laser deposited high temperature thin film sensors for gas turbines. *Aircr. Eng. Aerosp. Technol.* **2020**, *92*, 2–7. https://doi.org/10.1108/AEAT-11-2018-0292.
53. Feist, J. Luminescent Thermal History Sensors Fundamentals and Applications for Thermal Profiling. In Proceedings of the STO-MP-AVT-229—Test Cell and Controls Instrumentation and EHM Technologies for Military Air, Land and Sea Turbine Engines, NATO STO, Rzeszów, Poland, 20–23 April 2015; pp. 1–15.
54. Jenkins, T.P.; Hess, C.F.; Allison, S.W.; Eldridge, J.I. Measurements of turbine blade temperature in an operating aero engine using thermographic phosphors. *Meas. Sci. Technol.* **2020**, *31*, 044003. https://doi.org/10.1088/1361-6501/ab4c20.
55. Aust, J.; Pons, D.; Mitrovic, A. Evaluation of Influence Factors on the Visual Inspection Performance of Aircraft Engine Blades. *Aerospace* **2022**, *9*, 18. https://doi.org/10.3390/aerospace9010018.
56. Szczepankowski, A.; Przysowa, R. Thermal degradation of turbine components in a military turbofan. *Eng. Fail. Anal.* **2022**, *134*, 106088. https://doi.org/10.1016/j.engfailanal.2022.106088.
57. Bogdan, M.; Błachnio, J.; Kułaszka, A.; Zasada, D. Investigation of the Relationship between Degradation of the Coating of Gas Turbine Blades and Its Surface Color. *Materials* **2021**, *14*, 7843. https://doi.org/10.3390/ma14247843.
58. Kozakiewicz, A.; Jóźwiak, S.; Jóźwiak, P.; Kachel, S. Material Origins of the Accelerated Operational Wear of RD-33 Engine Blades. *Materials* **2021**, *14*, 336. https://doi.org/10.3390/ma14020336.
59. Kablov, E.; Muboyadzhyan, S.; Budinovskii, S.; Lutsenko, A. Ion-plasma protective coatings for gas-turbine engine blades. *Russ. Metall.* **2007**, *2007*, 364–372.
60. Yakovchuk, K.Y.; Rudoi, Y.É.; Onoprienko, E.V.; Malysheva, V.G. Effect of Protective Coatings on Mechanical Properties of ZhS32-VI Heat-Resistant Alloy. *Strength Mater.* **2010**, *42*, 352–361. https://doi.org/10.1007/s11223-010-9224-2.
61. Swadzba, L.; Maciejny, A.; Mendala, B. Overaluminising of NiCoCrAlY Coatings by Arc PVD on Ni-Base Superalloys. In Proceedings of the Superalloys 2000 (Ninth International Symposium), Champion, PA, USA, 17–21 September 2000; pp. 693–701. https://doi.org/10.7449/2000/Superalloys_2000_693_701.
62. Guo, X.; Zheng, W.; Xiao, C.; Li, L.; Antonov, S.; Zheng, Y.; Feng, Q. Evaluation of microstructural degradation in a failed gas turbine blade due to overheating. *Eng. Fail. Anal.* **2019**, *103*, 308–318. https://doi.org/10.1016/j.engfailanal.2019.04.021.
63. Wee, S.; Do, J.; Kim, K.; Lee, C.; Seok, C.; Choi, B.G.; Choi, Y.; Kim, W. Review on mechanical thermal properties of superalloys and thermal barrier coating used in gas turbines. *Appl. Sci.* **2020**, *10*, 5476. https://doi.org/10.3390/app10165476.
64. Chen, K.; Seo, D.; Canteenwalla, P. The Effect of High-Temperature Water Vapour on Degradation and Failure of Hot Section Components of Gas Turbine Engines. *Coatings* **2021**, *11*, 1061. https://doi.org/10.3390/coatings11091061.
65. Ułanowicz, L.; Dudziński, A.; Szczepaniak, P.; Nowakowski, M. Applying Protective Coating on the Turbine Engine Turbine Blades by Means of Plasma Spraying. *J. Konbin* **2020**, *50*, 193–213. https://doi.org/10.2478/jok-2020-0012.
66. Budinovskij, S.; Mubojadzhjan, S.; Gajamov, A.; Kos'min, A. Udalenie zharostojkih pokrytij s poverhnosti pera lopatok turbin v vodnyh malokoncentrirovannyh rastvorah (Removal of heat-resistant coatings from the surface of the turbine blade airfoil in aqueous low-concentrated solutions). *Tehnol. Met. (Met. Technol.)* **2006**, *11*, 40–45.
67. *Gazturbinny Dwigatel RD-33. Rukawodstwo po Techniczeskoj Ekspluatcji (RD-33 Gas-Turbine Engine. Technical Maintenance Manual) 0088.00.1700 RE*; Chernyshev Moscow Machine-Building Enterprise, Moscow, Russia, 2010; Volumes 1–4
68. Mentor Visual iQ VideoProbe Intelligent Inspection Solutions. Available online: https://www.everestvit.pl/images/pdf/Mentor-Visual-iQ-Everest-Waygate-03-2020.pdf (accessed on 6 March 2022).
69. Mentor Visual iQ VideoProbe User's Manual. Available online: https://www.instrumart.com/assets/MVIQ-manual.pdf (accessed on 6 March 2022).